Indian Journal of Engineering & Materials Sciences
Vol. 31, June 2024, pp. 450-458
DOI: 10.56042/ijems.v31i3.4463

A simplified approach to detect and diagnose the faults in pv array electricity generation system

Abhishek Kumar Gupta[a]*, Rajveer Singh[a] & Sanjiv Kumar[b]

[a]Department of Electrical Engineering, Jamia Millia Islamia, New Delhi 110025, India

[b]Department of Electrical Engineering, Government Polytechnic, Shahabad, Rampur U.P. 244922, India

Received: 31 July 2023; Accepted: 4 March 2024

Photovoltaic (PV) energy has become recognized as an important alternative energy source because of its efficient conversion method. Nevertheless, issues such as partial shade and faults can considerably diminish the power output of PV arrays, requiring the implementation of efficient fault detection and diagnosis methods to ensure safe and optimal operation. This article presents a simplified mathematical model for photovoltaic (PV) systems and proposes a fault detection method based on the use of solar irradiance, voltage, and current parameters. The system utilizes voltage and current ratios, together with irradiation data, to determine threshold values that can be used to diagnose different fault modes. The fault detection approach has been examined on a 4×4 PV array with a power capacity of 1600 W using MATLAB/Simulink R2019a. The method's accuracy has been verified by further experimental setups. The results demonstrate that the technique is uncomplicated, requires a smaller amount of data for identifying defects, and automatically characterizes faults with a high level of precision.

Keywords: Fault detection, Fault diagnosis, Photovoltaic array, Photovoltaic modeling, Partial shading, Wavelet packet transform

1 Introduction

Photovoltaic (PV) systems have recently emerged as a leading method of directly harnessing solar energy. Their popularity is expected to grow as technology advances, traditional energy sources become limited, and material costs drop. Reliable, safe, and efficient solar power plants require extensive fault analysis[1]. Unresolved faults can result in significant energy loss, system unreliability, and safety hazards, such as module failures and fire risks from DC arcing[2]. Historical incidents, such as the 2009 Bakersfield fire, highlight the need for effective fault detection and prevention mechanisms in PV systems[3]. Current protection devices, such as arc-fault circuit interrupters, over-current protection devices (OCPD), and ground fault protection devices (GFPD), are limited. They primarily operate under high current conditions and fail to address more complex fault scenarios, emphasizing the need for more sophisticated solutions[4].

Existing literature describes several fault detection methodologies that use I-V curve analysis and data-driven techniques. However, these approaches frequently necessitate large amounts of data and have high algorithmic complexity[5]. Artificial neural networks and fuzzy systems are frequently used to detect shading-related faults, but these methods typically focus on a narrow fault spectrum and require significant computational resources[6]. A new reconfiguration procedure has been proposed called two-phase array reconfiguration. According to the literature, artificial neural networks and fuzzy systems are commonly used techniques for detecting faults due to PV array shading[7]. The abnormal conditions in the photovoltaic system, like various faults and shading on PV cells, etc, are the primary cause of the depreciation of maximum power available at the PV terminals. Spataru *et al.*[8] proposed a fault diagnosis technique based on ensemble learning. Only two types of faults (short-circuit and partial shading) can be detected using this technique. Five parameters, like solar irradiation, cell temperature, ambiance temperature, output current, and output voltage of PV array, are required to diagnose the faults. Hariharan *et al.*[9] proposed a technique which analyzes the faults in two types only, i.e., permanent fault and partial shading. Furthermore, faults in aquatic PV modules, such as open-circuit faults caused by damaged cells and short-circuit faults from line-to-line or line-to-ground connections, pose unique challenges. Similarly, partial shading and degradation can result in significant power losses and black spots on modules, complicating

*Corresponding author (E-mail: akeed01@gmail.com)

fault detection even further. Thus, there is an urgent need for efficient, automated fault detection techniques that reduce data requirements and system complexity[10].

This paper presents a novel and simplified mathematical model for PV systems, along with an innovative fault detection and diagnosis algorithm. The proposed method automatically extracts relevant features and identifies faults in any segment of the PV array. Extensive evaluation with MATLAB/Simulink R2019a and experimental validation on a 4×4 PV array demonstrate the technique's effectiveness. It accurately identifies various faults, improving the reliability and safety of PV systems. This approach represents a significant advancement in fault detection technology, offering a more accessible and resource-efficient solution for maintaining PV array performance.

This study makes numerous important contributions. First, it provides a simplified mathematical model of PV systems to aid comprehension and application. Second, the developed fault detection and diagnosis algorithm can automatically extract features, allowing faults to be identified uniquely across the PV array. Third, the study contrasts the proposed method with existing fault detection techniques, emphasizing its superior efficiency and accuracy. The findings demonstrate that the proposed technique has the potential to significantly improve fault detection processes, paving the way for more resilient and safe PV installations.

2 Materials and Methods

2.1 Modelling of PV cell

The commonly used one-diode model of PV cells, shown in Fig. 1, is used for creating a photovoltaic array to examine various failures. A PV cell's equivalent circuit consists of a controlled current source known as photocurrent I_{ph}, an anti-parallel diode carrying current I_D, a shunt resistance R_{sh}, and a series resistance R_s. I_{sh} denotes the current in shunt resistance.

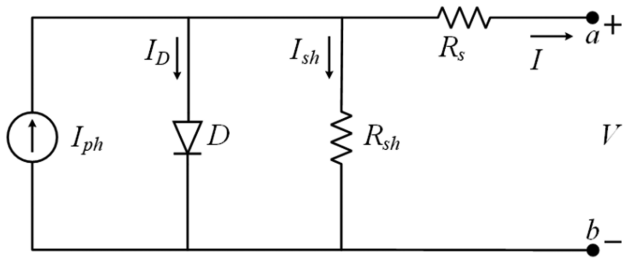

Fig. 1 — Equivalent circuit of one diode model of PV cell.

The current source in the equivalent circuit depends on the solar irradiance and the cell temperature given by Equation (1)[11]:

$$I_{ph} = \left(I_{ph,n} + K_I \Delta T\right) \frac{G}{G_n} \quad ...(1)$$

where, $I_{ph,n}$ is the short-circuit current, K_I is the temperature coefficient of short circuit current.G and G_n are the instantaneous and nominal irradiance respectively. The relative temperature is given by:

$$\Delta T = T - T_n \quad ...(2)$$

where, T is instantaneous temperature and T_n is the nominal temperature. The equation for the antiparallel diode (D)in Fig. 1 is given by (3):

$$I_D = I_s \left[e^{\left(\frac{qV_d}{AkT}\right)} - 1\right] \quad ...(3)$$

where, $I_s$is the reverse saturation current, q is the electron charge (q = 1.60217646×10^{-19} C), VD is diode voltage, A is the linearity factor (ideally 1), k is Boltzmann constant (k = 1.3806503×10^{-23} J/K) and T is absolute temperature in Kelvin. The PV cell current at load terminal a-b of Fig. 1 can be written using the Kirch offs current law:

$$I = I_{ph} - I_D - I_{sh} \quad ...(4)$$

If there is series resistance R_s, then the diode current will be:

$$I_D = I_s \left[e^{\left(\frac{qV + R_S I)}{AkT}\right)} - 1\right] \quad ...(5)$$

Since, the current through shunt resistance is

$$I_{sh} = \frac{V + R_S I}{R_{sh}} \quad ...(6)$$

where V is the PV cell terminal voltage. Combining the equations, PV current I can be written as:

$$I = I_{ph} - I_s \left[e^{\left\{\frac{q(V + R_S I)}{AkT}\right\}} - 1\right] - \frac{V + R_S I}{R_{sh}} \quad ...(7)$$

The shunt branch in the PV cell equivalent circuit exists as a result of the leakage current. Because the R_{sh} used is very high so, the final term in (7), which is the current in the shunt branch (I_{sh}), can be ignored for simplicity. The exponential term in (7) second term is far greater than one. As a result, ignoring the term '-1' will have no effect on PV cell behavior. So, (7) can be written as:

$$I = I_{ph} - I_s e^{\left[\frac{q(V+R_S I)}{AkT}\right]} \quad \ldots(8)$$

Let, $C = \frac{q}{AkT}$ then,

$$I = I_{ph} - I_s e^{[(V+R_S I)C]} \quad \ldots(9)$$

With the help of (9), the photovoltaic cell's electrical characteristics can be determined. The variables I_{ph}, I_s, C, and R_s is to be determined from (9) with the help of the known parameters of PV cells like MPP voltage (V_{mpp}), MPP current (I_{mpp}), SC current (I_{sc}) and OC voltage (V_{oc}).When the load terminal is short-circuited, then:

$$I_{sc} = I_{ph} - I_s e^{(R_s I_{sc})C} \quad \ldots(10)$$

When the load terminal is open-circuited, then:

$$0 = I_{ph} - I_s e^{V_{oc}\,C} \quad \ldots(11)$$

And if the PV cell is operating at MPP, then:

$$I_{mpp} = I_{ph} - I_s e^{(V_{mpp}+R_s I_{mpp})C} \quad \ldots(12)$$

$$\left(\frac{dP}{dV}\middle|_{I=I_{mpp}}^{V=V_{mpp}}\right) = 0 \quad \ldots(13)$$

The cell parameters I_{ph}, I_s, C, and $R_s$can be obtained using the above equations. The solutions are obtained as:

$$C = \frac{I_{mpp}}{V_{mpp}(I_{ph}-I_{mpp})} \quad \ldots(14)$$

$$I_{ph} = I_{sc} + I_s e^{(R_s I_{sc})C} \quad \ldots(15)$$

$$I_s = e^{[log(I_{ph})-V_{oc}C]} \quad \ldots(16)$$

$$R_s = \frac{log\left(\frac{I_{ph}-I_{mpp}}{I_{ph}}\right) - C(V_{oc}-V_{mpp})}{I_{mpp}C} \quad \ldots(17)$$

Hence, using the above assumption, the ideality factor can be obtained for standard test conditions as well as for normal operating cell temperature.

$$A_{NOCT} = \frac{q}{C_{NOCT}T_{NOCT}k} \quad \ldots(18)$$

$$A_{STC} = \frac{q}{C_{STC}T_{STC}k} \quad \ldots(19)$$

STC and *NOCT* represent standard test conditions and normal operating cell temperatures, respectively.

2.2 Simulink model of 4×4 PV array

Figure 2 shows a PV array with four parallel and four series modules, which is modeled in MATLAB R2019a for further fault detection and diagnosis. The electrical specifications of a single PV module are shown in Table 1. The proposed model is tested under a various of environmental scenarios. Figures 3 and 5 show the proposed model's power-voltage (P-V) and current-voltage (I-V) characteristics under various

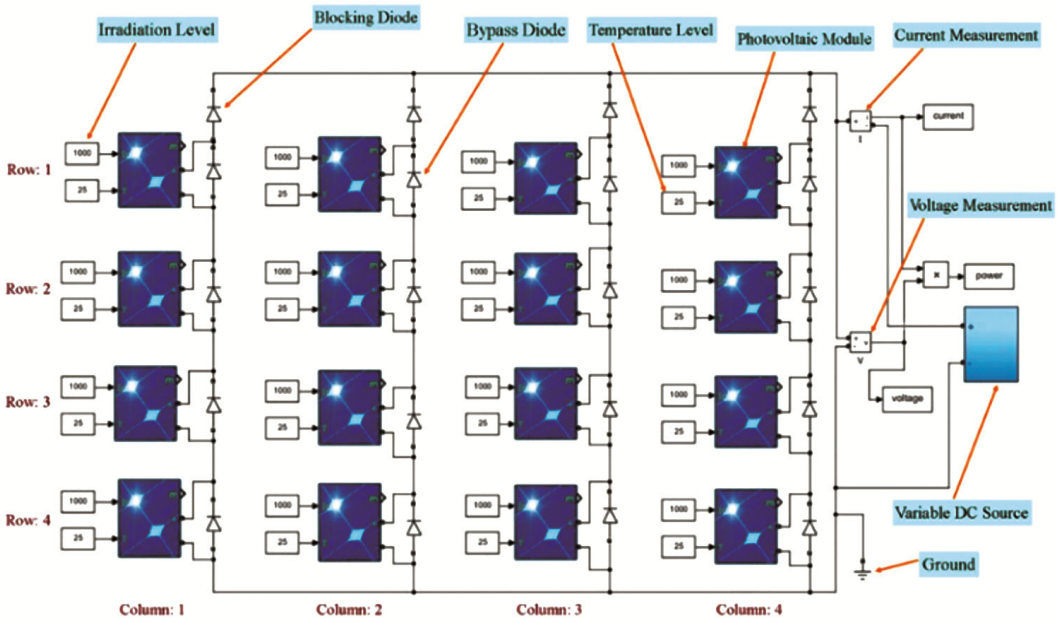

Fig. 2 — Simulink model of 4×4 solar PV system.

irradiation conditions. Both PV module characteristics under irradiance variation show that the maximum power point (MPP) of the PV array is directly proportional to the irradiation level on the PV module's surface. Similarly, the P-V and I-V characteristics of the proposed module are plotted under varying temperature conditions, as shown in Fig. 4 and Fig. 6, and it is found that the MPP of the PV array is inversely proportional to the temperature of the PV module.

Table 1 — Nexpower Technology NH-100 UT_4A solar panel electrical specification at STC

Parameter	Value
Maximum output power	100 W
Voltage at MPP (V_{mpp})	18 V
Current at MPP (I_{mpp})	5.56 A
Open-circuit voltage (V_{oc})	22 V
Short-circuit current (I_{sc})	6.06 A
Temperature coefficient of V_{oc}	-0.34 %/ °C
Temperature coefficient of I_{sc}	0.06 %/ °C
Shunt resistance (R_{sh})	81.34 ohm
Series resistance (R_{se})	0.24 ohm

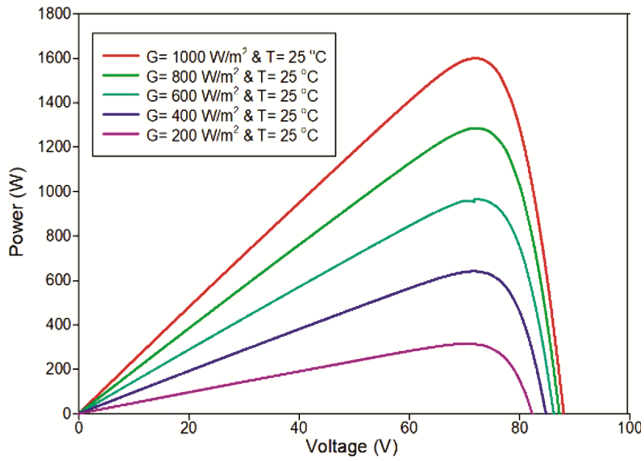

Fig. 3 — P-V curve at different irradiance.

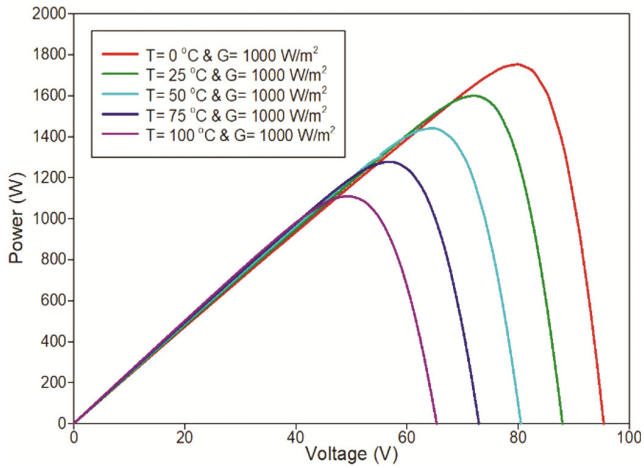

Fig. 4 — P-V curve at different temperatures.

2.3 Characterization of PV array under various faults

In solar photovoltaic array system the faults can be classified in two major catagories like permanent faults and temporary faults. The permanent faults in photovoltaic arrays are line-line, line-ground, mismatch, and open-circuit. These faults cause a permanent reduction in photovoltaic power generation. Temporary faults can include partial shading of the PV array. Line-line (LL) and line-ground (LG) faults occur as a result of an unintentional interaction between one or more lines of a photovoltaic array and ground, i.e., short-circuiting of two nodes with different potentials. Various faults in the photovoltaic array can be seen in Fig. 7. F_{LL1} and F_{LL2} are LL faults with mismatched one and two modules respectively. F_{LG1} and F_{LG2} represent LG and

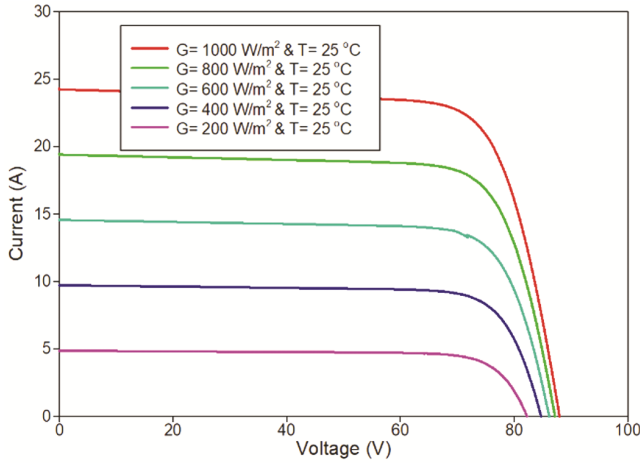

Fig. 5 — I-V curve at different irradiance.

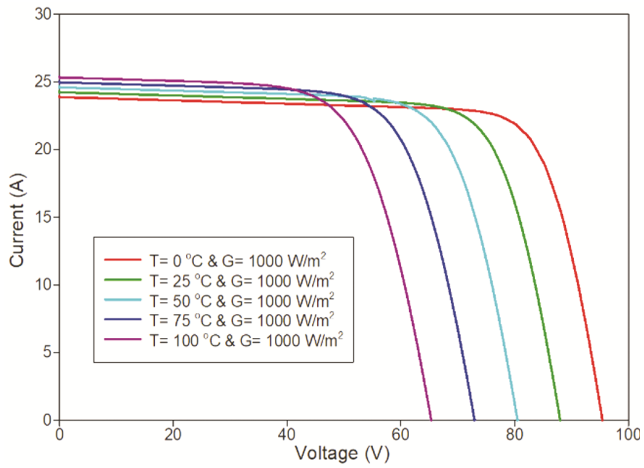

Fig. 6 — I-V curve at different temperatures.

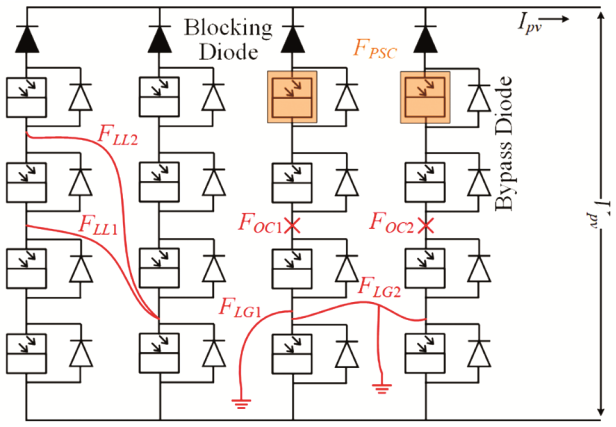

Fig. 7 — A 4×4 photovoltaic array with common faults.

LLG faults, respectively. F_{OC1} is an open-circuit fault in the third column, while F_{OC2} is an open-circuit fault in the fourth column. Based on the proposed model of photovoltaic cell, an array of 16 photovoltaic modules (4 parallel and 4 series) has been modeled in MATLAB/Simulink. The PV module specification is listed in Table 1. The array's maximum output power is 1600 W.

For the purpose of developing a faults detection and diagnosis algorithm, this paper takes into consideration the common faults, including line-line, line-ground, open-circuit, and shading faults, that are associated with the photovoltaic array system shown in Fig. 2. Both the voltage ratio (α) and the current ratio (β) are introduced in order to facilitate the detection of faults. A definition of the ratios α and β is as follows:

$$\alpha = \frac{V}{V_{oc}} \quad \ldots(20)$$

$$\beta = \frac{I}{I_{sc}} \quad \ldots(21)$$

where V_{oc} and I_{sc} are the voltage and current parameters at no-load and short-circuit conditions, respectively. The V_{oc} and I_{sc} can be obtained by[12]:

$$I_{sc} = N_p \left[\frac{I_{scSTC}}{1000} G + K_I(T - T_{STC})\right] \quad \ldots(22)$$

$$V_{oc} = N_s[V_{ocSTC} + K_V(T - T_{STC}) + V \ln\left(\frac{I_{sc}/N_p}{I_{scSTC}}\right)] \quad \ldots(23)$$

where, I_{scSTC}= short circuit current at STC, V_{ocSTC}= open-circuit voltage at STC, K_I= temperature coefficient of I_{sc}, K_V= temperature coefficient of V_{oc}, T_{STC}= temperature at STC (25 ^{O}C), N_p= number of PV modules connected in parallel, N_s= number of PV modules connected in parallel. The PV output parameters are lesser dependent on temperature variations compared to irradiation variations, so Equation (22) and (23) can be rewritten as:

$$I_{sc} = N_p \left[\frac{I_{scSTC}}{1000} G\right] \quad \ldots(24)$$

$$V_{oc} = N_s[V_{ocSTC} + V \ln\left(\frac{I_{sc}/N_p}{I_{scSTC}}\right)] \quad \ldots(25)$$

From Equation (20) and (21), if the PV system is operating in healthy condition, then the voltage and current ratios can be written as:

$$\alpha_{\mathrm{m}} = \frac{V_{mpp}}{V_{oc}} \quad \ldots(26)$$

$$\beta_{\mathrm{m}} = \frac{I_{mpp}}{I_{sc}} \quad \ldots(27)$$

In a healthy PV array, the V_{mpp} and I_{mpp} can be obtained as follows:

$$I_{mpp} = N_p \left[\frac{I_{mpSTC}}{1000} G + k_i(T - T_{STC})\right] \quad \ldots(28)$$

$$V_{mpp} = N_s \left[V \ln\left(1 + \left(\frac{I_{sc} - I_{mpp}}{I_{sc}}\right)\left(e^{\frac{V_{oc}}{N_s V_t}} - 1\right)\right) - \frac{I_{mpp}}{N_p} R_s\right] \quad \ldots(29)$$

2.4 Determination of Threshold Values

The threshold values are determined by the two specified variables, α and β (section 2.3). This part discusses the threshold values for different faults in PV arrays, such as line-line fault, line-ground fault, open-circuit fault, and partial shading.

2.4.1 LL and LG faults

In a grounded system, the LL faults and the LG faults behave identically. Furthermore, the PV parameter variations are identical for LL and LG faults[2]. When a line-line fault occurs in a PV string, the decrease in output voltage is proportional to the number of mismatched modules. Similarly, line-ground faults are determined by the voltage between the fault point and ground on the module. To calculate the voltage ratio for LL/LG faults ($\alpha_{LL/LG}$), use the following equation:

$$\alpha_{\mathrm{LL/LG}} = \left(1 - \frac{1}{\mathrm{N_s}}\right)\frac{V_{mpp}}{V_{oc}} = \gamma\alpha_{\mathrm{m}} \quad \ldots(30)$$

where, $\gamma = 1 - \frac{1}{\mathrm{N_s}}$. Hencethreshold value for the detection of faults in the case of LL/LG faults ($Th_{LL/LG}$) is given by:

$$Th_{LL/LG} = \gamma\alpha_{\mathrm{m}} \pm \varepsilon \quad \ldots(31)$$

Where ε is the percentage threshold range, $\varepsilon = \pm 2\%$.Hence, from (31)$Th_{LL/LG} = 0.5569 \pm \varepsilon$

2.4.2 Open circuit faults

In the occurrence of an open-circuit fault in a PV string, the reduced output current is proportional to the current of the faulty line. The current ratio for open circuit faults (β_{oc}) can be calculated as follows:

$$Th_{oc} = \lambda \beta_m \pm \varepsilon = 0.6045 \pm \varepsilon \quad \ldots(33)$$

where, $\lambda = 1 - \frac{1}{N_p}$. Hencethreshold value for the detection of faults in the case of open-circuitfaults (Th_{OC}) is given by:

$$\beta_{oc} = \left(1 - \frac{1}{N_p}\right)\frac{I_{mpp}}{I_{sc}} = \lambda\, \beta_m \quad \ldots(32)$$

2.4.3 Partial shading faults

The partial shading fault is considered a temporary fault. Such faults are common in PV generation systems. The shaded cell produces less current, so the module generates less power than other modules. In this case, the voltage and current ratios are calculated as follows:

$$\alpha_{PSC} = \frac{V_{mp}}{V_{oc}} \quad \ldots(34)$$

$$\beta_{\mathrm{PSC}} = \frac{\mathrm{I_{mp}}}{\mathrm{I_{sc}}} \quad \ldots(35)$$

In case of partial shading the V_{mp} and I_{mp} are the MPP values from the photovoltaic array with peak irradiation (G_{mp}). Hence, the V_{mp} and I_{mp} for partial shading can be obtained the same as (28) and (29) by replacing G by G_{mp}, V_{mpp} by V_{mp} and I_{mpp} by I_{mp}.Hence, the threshold value for the detection of faults in the case of partial shading faults is given by:

$$Th_{PSC} = \left(\frac{I_{mp}}{I_{sc}}\right) \pm \varepsilon = k\left(\frac{I_{mpp}}{I_{sc}}\right) \pm \varepsilon = \beta_{PSC} \pm \varepsilon = 0.5239 \pm \quad \ldots(36)$$

where k is the irradiation factor and based on the peak irradiation, the value of k ranges from 0.4 to 0.7.

A flowchart has been developed based on the discussed threshold values, shown in Fig. 8.

3 Results and Discussion

3.1 Simulation results

To get the results of the proposed fault detection technique, a PV generation system with 1600 W is developed on MATLAB/Simulink R2019a. The structure of the modeled system is shown in Fig. 2. The electrical parameters of the PV module are given in Table 1.

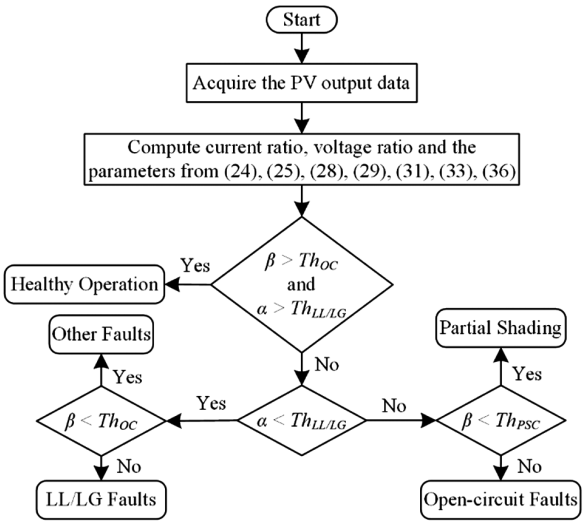

Fig. 8 — Flow chart of the proposed technique of photovoltaic faults characterization and detection

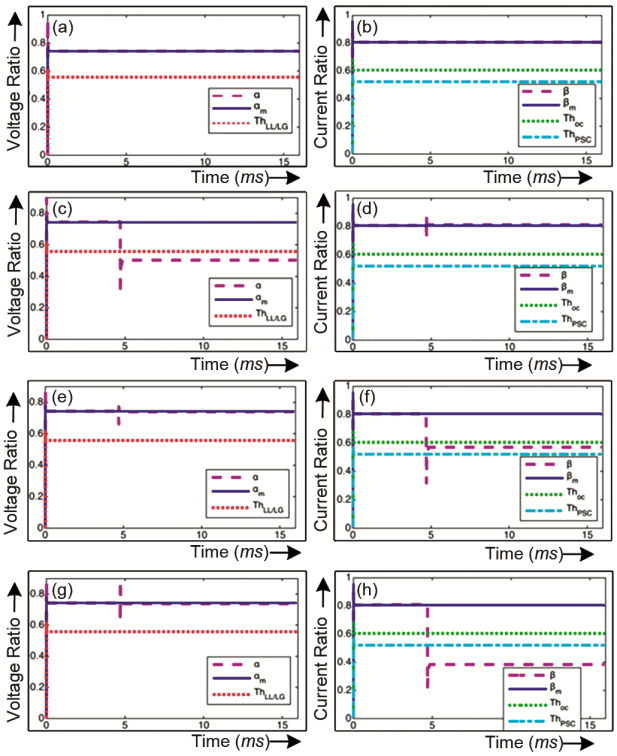

Fig. 9 — (a) Voltage ratio duringhealthy operation, (b) current ratio during healthy operation, (c) voltage ratio during LL/LG fault, (d) current ratio during LL/LG fault, (e) voltage ratio during open-circuit fault (f) current ratio during open-circuit fault, (g) voltage ratio during PSC, and (h) current ratio during PSC

3.1.1Healthy operation

Healthy operation of the PV system is highly desirable. Figure 9 (a) and (b) show the voltage and current parameter ratios for a healthy operation

respectively. During this observation, the test conditions were 25°C temperature and 1000 W/m^2 irradiation. Figure 9 (a) displays voltage ratios (α and α_m) and the threshold for LL/LG faults ($Th_{LL/LG}$). Fig. 9 (b) displays the current ratios (β and β_m), as well as the thresholds for OC and PSC faults (Th_{OC} and Th_{PSC}). $Th_{LL/LG}$ is lower than α, indicating that the PV system is not experiencing any LL/LG faults. β exceeds Th_{OC} and Th_{PSC}, indicating that the PV system is free of open circuit faults and partial shading.

3.1.2 During line-line/line-ground fault

In Fig. 7, F_{OC1} and F_{OC2} displays an open-circuit faults in photovoltaic strings 3 and 4, respectively. Figure 9 (c) and (d) show the voltage and current ratios with their corresponding thresholds respectively during LL/LG fault operation. LL/LG faults are the unusual connection between two or more different potential nodes, so in such cases, the voltage of the photovoltaic system decreases. The voltage of the PV string is reduced by the summation of the voltages of the mismatched photovoltaic modules. So, $\alpha$is lower than the $Th_{LL/LG}$ as shown in Fig. 9 (c), i.e. the PV array is operating under LL/LG fault. Fig. 9 (d), shows that the PV system is free from the open circuit and partial shading faults.

3.1.3 During open-circuit fault

In Fig. 7, F_{LL1},and F_{LL2} shows the line-line faults, and F_{LG1} and F_{LG2}shows line-ground faults. Figure 9 (e) and (f) show the voltage and current ratios with their corresponding thresholds respectively during open circuit fault operation. Since, α is greater than $Th_{LL/LG}$ during operation. So, the PV system is free of LL/LG faults. β is less than Th_{OC} and greater than Th_{PSC}, indicating an open-circuit fault in one of the PV strings.

3.1.4 During partial shading condition

In the case of partial shading, some part of the photovoltaic array is shaded for some time by any means, and the rest gets the total available irradiation, as shown in Fig. 7 indicated by F_{PSC}. The shading pattern considered for partial shading of the PV array is given in Table 2. Figure 9 (g) shows, α is greater than the $Th_{LL/LG}$ during the operation. So, the PV system is free from LL/LG faults. In Fig. 9 (h), β is less than the Th_{OC} as well as Th_{PSC}, means the PV system is operating in the partial shading condition.

The percentage error can be calculated as the difference between the threshold value and the corresponding fault parameter multiplied by one hundred. Similarly, the corresponding accuracy index can be assessed. The evaluation index for the fault cases LL/LG fault, open-circuit fault, and partial shading fault are 90.18%, 94.29%, and 73.33%, respectively overall efficiency of the proposed system is the average efficiency, i.e., 85.93%.

3.2 Experimental results

The proposed technique has also been implemented on the hardware. The experimental setup for validating the proposed method is shown in Fig. 10 (a) and (b). The electrical parameters of the solar PV panel used in the experimental setup at standard test conditions (irradiation = 1000 W/m^2 and temperature = 25 ^{o}C) are as follows: nominal power = 100 W, open-circuit voltage = 50.5 V, short-circuit current = 3.3 A, voltage at MPP = 37.5 V, current at MPP = 2.66 A.

The gating signal for the boost converter is generated using LAUNCHXL-F28379D and MATLAB/

Table2 — Sample shading pattern

	Irradiation Level (W/m^2)			
Row 1	1000	1000	1000	1000
Row 2	1000	1000	1000	1000
Row 3	800	800	800	800
Row 4	700	700	700	700

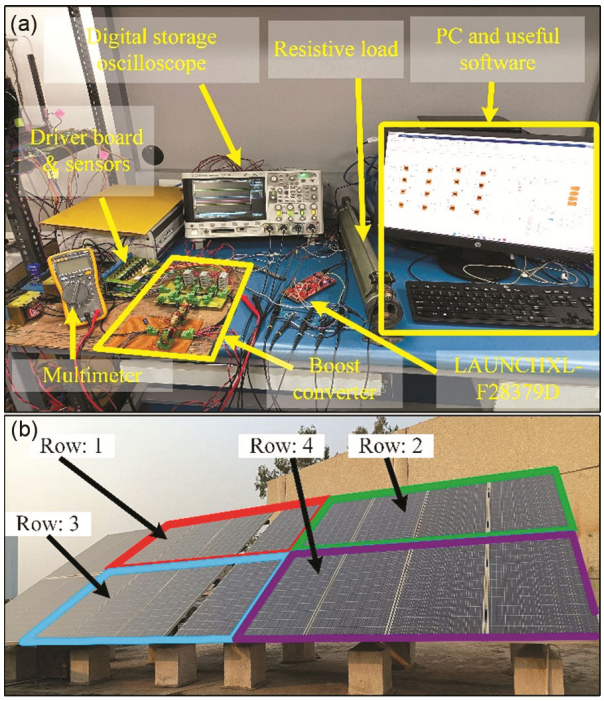

Fig. 10 — Experimental setup (a) computer with LAUNCHXL-F28379D, Boost converter, Oscilloscope, Multimeter, Resistive load, and (b) Roof-top solar PV array

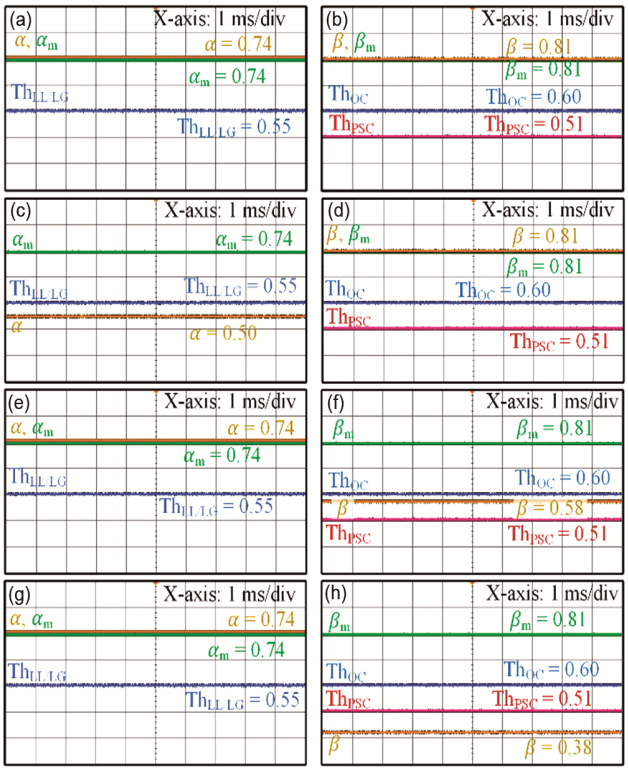

Fig. 11 — Experimental results (a) voltage ratio during healthy operation, (b) current ratio during healthy operation, (c) voltage ratio during LL/LG fault, (d) current ratio during LL/LG fault, (e) voltage ratio during open-circuit fault, (f) current ratio during open-circuit fault, (g) voltage ratio during PSC, and (h) current ratio during PSC.

Simulink 2021a. Since the proposed algorithm requires voltage and current inputs, sensors are used to sense the real-time voltage and current for the ADC pin of the controller. A DSO-X 2014A digital storage oscilloscope is used to record and capture the results. The roof-top solar PV array shown in Fig. 10 (b) is connected in four columns with four PV modules in series in each column. The experimental results for validation of the proposed fault detection algorithm are shown in Figs. 11 (a–h). In healthy condition, $\alpha > Th_{LL/LG}$ and $\beta > Th_{OC}$ & Th_{PSC} shown in Fig. 11 (a) and (b). An LL fault is created with one module mismatch, in this case $\alpha < Th_{LL/LG}$ and $\beta > Th_{OC}$ & Th_{PSC} shown in Fig. 11 (c) and (d). To validate algorithm for open-circuit fault, an open circuit is created in string 3 of the PV array shown in Fig. 2, in this case $\alpha > Th_{LL/LG}$ and $Th_{PSC} < \beta < Th_{OC}$ shown in Fig. 11 (e) and (f). The algorithm is tested for the partial shading condition for theirradiation pattern given in Table 2. In this case $\alpha > Th_{LL/LG}$ and $\beta < Th_{OC}$ & Th_{PSC} both shown in Fig. 11 (g) and (h). Table 3 summarizes and presents the simulation results for the fault variable.

4 Conclusion

In the first part of section 2 a simplified modelling of PV cell is presented and in the second part a fault ditection and characterization technique for PV array is proposed. The proposed fault detection method is

Table 3 — PV fault parameters under different fault conditions

Types of faults	Simulation results				Experimental Results			
	α	β	err (%)	η (%)	α	β	err (%)	η (%)
LL/LG fault	0.5022	0.8113	9.82	90.18	0.50	0.81	10.22	89.78
Open-circuit fault	0.7393	0.5700	5.71	94.29	0.74	0.58	4.05	95.95
Partial shading fault	0.7373	0.3842	26.67	73.33	0.74	0.38	27.47	72.53

Table 4 — Comparison with the recent PV faults detection techniques

Reference	Fault Type	Method	Parameters Required	Accuracy	Complexity
Hariharan *et al.*[9]	Permanent fault, Partial shading	Difference Measurement	V, I, G	High	High
Chen *et al.*[11]	Short circuit, Open circuit, Partial shading, Degradation	Machine Learning	V, I, G, T	High	High
Dhimish*et al.*[13]	PV module fault, Partial shading, MPPT Fault	Difference Measurement	V, I, G, T	Low	High
Kumar *et al.*[14]	LL fault, Partial shading	Signal Processing	V, I, G	High	Low
Huang *et al.*[15]	LL fault, Partial shading, Abnormal aging	Machine Learning	V, I, G, T	High	High
Liu *et al.*[16]	LL fault, Partial shading, Degradation, Bypass diode fault	Machine Learning	V, I, G	High	High
Proposed Algorithm	LL/LG fault, Open circuit fault, Partial shading	Difference Measurement	V, I, G	High	Low

based on some basic electrical parameters such as the PV array's voltage, current, and irradiance data, which means that the fault detection system only needs three sensors to accurately detect and identify the fault. The proposed flowchart in Fig. 8 is useful for identifying the types of faults that occurred at the PV array, including LL/LG (short-circuit) faults, open-circuit faults, and partial shading. The developed MATLAB/Simulink photovoltaic generation model was tested under a variety of environmental conditions. Different faults were considered and used for fault analysis, detection, and identification. This fault detection algorithm was applied to the modeled PV generation system, and it was found that the proposed fault detection technique is capable of accurately detecting and identifying faults with only three input data points, namely voltage, current, and irradiance on the PV module surface. The fault detection algorithm is validated using the experimental setup. Table 3 summarizes the accuracy of the proposed fault detection technique in both simulation and experimental cases. The proposed method was also compared to the various PV fault detection techniques available in the literature, as illustrated in Table 4. The proposed PV fault detection technique is simple, efficient, and requires a minimal amount of data to detect and characterize the faults.

References

1 Gupta A K, Singh R & Kumar S, *Trans Indian Natl AcadEng*, 8 (2023) 607.
2 Zhao Y, Palma J F de, Mosesian J, Lyons R & Lehman B, *IEEE Trans Ind Electron*, 60 (2013) 3784.
3 Falvo M C &Capparella S, *Case Stud Fire Saf*, 3 (2015) 1.
4 U.S. National Electrical Code, *Art 690 - Solar PV Systems*, (2014) 623.
5 Fadhel S, Delpha C, Diallo D, Bahri I, Migan A, Trabelsi M & Mimouni M F, *Sol Energy*, 179 (2019) 1.
6 Olabi A G, Abdelkareem M A, Semeraro C, Al Radi M, Rezk H, Muhaisen O, Al-Isawi O A & Sayed E T, *Thermal Sci Eng Prog*, 37 (2023) 101612.
7 Dhimish M, Holmes V, Mehrdadi B & Dales M, *Electr Power Syst Res*, 151 (2017) 26.
8 Spataru S, Sera D, Kerekes T & Teodorescu R, *Sol Energy*, 119 (2015) 29.
9 Hariharan R, Chakkarapani M, Ilango G S, Nagamani C & Member S, *IEEE J Photovoltaics*, 6 (2016) 1278.
10 Osmani K, Haddad A, Lemenand T, Castanier B, Alkhedher M & Ramadan M, *Energy Nexus*, 12 (2023) 1.
11 Chen Z, Wu L, Cheng S, Lin P, Wu Y & Lin W, *Appl Energy*, 204 (2017) 912.
12 Silvestre S, Da Silva M A, Chouder A, Guasch D & Karatepe E, *Energy Conv Manag*, 86 (2014) 241.
13 Dhimish M, Holmes V, Mehrdadi B & Dales M, *IET Renew Power Gener*, 11 (2017) 1565.
14 Kumar B P, Ilango G S, B. Reddy M J & Chilakapati N, *IEEE J Photovolt*, 8 (2018) 257.
15 Huang J M, Wai R J & Gao W, *IEEE Access*, 7 (2019) 70919.
16 Liu Y, Ding K, Zhang J, Li Y, Yang Z, Zheng W & Xhen X, *Energy Conv Manag*, 245 (2021) 1.